# Usefulness of Iodine-Blood Material Density Images in Estimating Degree of Liver Fibrosis by Calculating Extracellular Volume Fraction Obtained from Routine Dual-energy Liver CT Protocol Equilibrium Phase Data: Preliminary Experience

**Emi Ito[1] · Keisuke Sato[1] · Ryotaro Yamamoto[2] · Keiko Sakamoto[1] · Hiroshi Urakawa[1] · Kengo Yoshimitsu[1]**

**(Keisuke Sato and Ryotaro Yamamoto are equivalent first authors, contributing as equally as the first author Emi Ito.)**

[1] **Department of Radiology, Faculty of Medicine, Fukuoka University, 7-45-1 Nanakuma, Jonan-ku, Fukuoka 814-0180, Japan**

[2] **Department of Radiology, Fukuoka University Chikushi Hospital, 1-1-1 Zokumyoin, Chikushino, Fukuoka 818-8502, Japan**

**ABSTRACT**

PURPOSE: To assess whether extracellular volume fraction (ECV) calculated from iodine(-blood) density images (I-B) of dual-energy liver CT (DECT) equilibrium phase data (EqD) is useful in estimating the degree of liver fibrosis.

MATERIALS AND METHODS: Consecutive 52 patients with chronic liver disease who underwent fast kV switching DECT and liver MR elastography (MRE) were retrospectively enrolled. Iodine(-water) density images (I-W) and I-B were generated from EqD and ECV were calculated. As blood pools, abdominal aorta (Ao) and suprahepatic inferior vena cava (IVC) were chosen, and therefore 4 types of ECV ($ECV_{\text{I-W Ao}}$, $ECV_{\text{I-W IVC}}$, $ECV_{\text{I-B Ao}}$, $ECV_{\text{I-B IVC}}$) were obtained. ECV was also calculated using conventional method ($ECV_{\text{conv Ao}}$). The correlation coefficients ($R^2$ or rho) of these five ECVs versus liver stiffness (MRE) or pathologically proven fibrosis grades were compared.

RESULTS: As for correlation with liver stiffness, $R^2$ for $ECV_{\text{conv.Ao}}$, $ECV_{\text{I-W Ao}}$, $ECV_{\text{I-B Ao}}$, $ECV_{\text{I-W IVC}}$, and $ECV_{\text{I-B IVC}}$, were 0.26, 0.34, 0.44, 0.39, and 0.52, respectively (all $p<0.0001$). Histopathological correlation was available in 28 patients, and rho values were 0.61, 0.60, 0.71, 0.68, and 0.76, respectively (all $p<0.001$).

CONCLUSION: $ECV_{\text{I-B IVC}}$ calculated from EqD of DECT is useful in estimating the degree of liver fibrosis.

## Introduction

Assessment of the degree of liver fibrosis is important in the management of patients with chronic liver disease, because it has been shown to be related to the prognosis of these patients directly or indirectly via hepatocarcinogenesis [1–4]. Several imaging approaches have been reported to be useful as tools for non-invasive assessment of liver fibrosis, including shearwave or strain ultrasonographic elastography, or MR elastography (MRE) [3, 4]. Among these, MRE may be the most reliable and accurate, according to the recently accumulated evidences [3–5]. However, all these methods are additional examination to the routine clinical follow up, or require specific hardware and/ or software.

Assessment of liver fibrosis degree by estimating extracellular volume fraction (ECV) has been attempted utilizing the equilibrium phase of contrast-enhanced CT [6–9]. ECV in % is simply expressed as (100 hematocrit) *Δ liver /Δ blood pool, where Δ represents the difference in the CT values between the unenhanced and equilibrium phases, because the concentration of iodine is considered the same for both intra- and extra-vascular spaces at the equilibrium phase [6–9]. ECV is the sum of extracellular extravascular space and intravascular space of a tissue; the former is the place where fibrosis occurs, whereas the latter is not [6, 7]. In spite of the unknown factor of intravascular space included, an initial animal study showed very high correlation between ECV and quantitatively assessed pathological fibrosis volume [6], followed by several clinical studies with promising results [7–9]. Recently reported was a high accuracy of ECV in discriminating early from advanced stage liver fibrosis using precise subtraction algorithm and 240 s equilibrium phase clinical CT data [10].

ECV was originally calculated by manually placed region of interests (ROI) both on the unenhanced and equilibrium phase images [6–8], but with the advent of dual-energy CT (DECT) technology, the concept of materials decomposition images with an iodine–water materials basis pair has been introduced, which simply enables quantification of iodine

(iodine(-water) density image) [11, 12]. Theoretically speaking, ECV can be obtained solely from this iodine(-water) density image of equilibrium phase data without the need to subtract unenhanced image information from the equilibrium phase information. There are several benefits to this single (dual energy) acquisition, such as reduced radiation by omitting unenhanced scanning, and no anatomical misregistration between unenhanced and equilibrium phase images. One concern in this setting, however, is possible inaccuracy in the iodine quantification due to the use of "water" as one of the basis materials. For example, because this concept is based on an assumption that any materials are made up of iodine and water, the value of the blood pool, typically the abdominal aorta (Ao), on the iodine(-water) density images before contrast enhancement, exhibits some positive values, which is theoretically supposed to be zero. This erroneously suggests the presence of some amount of iodine in the aorta before contrast administration, possibly leading to inadequate ECV calculation. To solve this problem, we proposed to use iodine(-blood) density imaging, instead of iodine(-water), namely using iodine and blood as two basis materials. Another concern we noticed was the apparent streaking artefacts around the vertebral body on the iodine density images, typically overlapping on the abdominal aorta, which could degrade the blood pool measurement, and resultantly ECV assessment, as well. To avoid this problem, we proposed to use inferior vena cava (IVC) just above the hepatic dome for blood pool measurement, which is at a further distance from the vertebral bodies and, therefore, less subject to the artifacts than the aorta. Thus, there are four types of iodine density map-derived ECVs to be tested, based on combination of the two iodine material density images (water vs blood), and two blood pools (Ao vs IVC).

The purpose of this study is to elucidate whether any one of the four ECVs obtained from routine liver DECT equilibrium phase image data is useful in estimating the degree of liver fibrosis, as compared to the one calculated by the conventional manual ROI method.

## Materials and methods

### *Patients*

Between April 2016 and March 2017, consecutive 52 patients with chronic liver disease who underwent both quadri-phase DECT and MRE within 3 months were retrospectively recruited. Flowchart of patient selection is shown in Fig. 1. There were 26 men and 26 women, with age ranging from 35 to 88 years (average 67), all of whom had had suspected liver masses on ultrasonography. The demographic data of these patients are shown in Table 1. Our institutional review board waived obtaining informed consent from the patients for this study because of its retrospective nature.

### *CT protocol*

CT equipment used was a 64-row DECT (Discovery CT750 HD, GE Healthcare, Milwakee, USA), and scanning parameters were as follows: detector configuration 64 × 0.625, tube voltage 80/140 kV, tube current 640 mA, gantry revolution time 0.6 s, acquisition mode helical, helical pitch 1.375, field of view 50 cm, volume CT dose index 15.6 mGy, reconstruction thickness 5 mm, reconstruction increment 5 mm, reconstruction algorithm projection-based material decomposition, reconstruction kernel soft tissue. All four phases were obtained with dual-energy mode. After obtaining unenhanced images, 600 mgI/kg iodine contrast medium (Iopamiron 370, Bayer Health Care, Osaka, Japan) was injected for 30 s at a variable injection rate, and arterial dominant phase images were obtained using bolus tracking method, followed by portal dominant phase at 60 s, and equilibrium phase images at 240 s after the commencement of contrast medium injection.

Iodine(-water) and iodine(-blood) density images were generated using the dedicated application “GSI viewer” (GE Healthcare, Milwakee, USA) installed within the CT console. To generate iodine(-blood) density map, information of “blood”, including mass attenuation coefficient, should be given as input into GSI viewer, which can be obtained from the site of National Institute of Standards and Technology (NIST) [13].

*MRE protocol*

MRE was obtained with a 3.0 T clinical unit (Discovery 750 W, GE, Milwaukee, USA) along with a 32-element phased-array coil. A 19-cm-diameter passive pneumatic driver was positioned over the center of the right rib cage at the level of the xiphoid process and attached to an acoustic waveform generator. A 60-Hz waveform was applied to the driver. A 2D spin-echo echo-planar MRE sequence (TR/TE=1000/59, 66×64 matrix, 10 mm slice thickness, 80-Hz magnetization encoding gradient) acquired magnitude and unwrapped phase difference wave images using a 42-cm field of view [6, 14, 15]. Four slices were obtained including the level of the hepatic hilum under 16-s breath holding. Wave images and MRE images (stiffness map) with crosshatching marks were automatically generated on the operating console. The inversion algorithm used for stiffness map calculation was a multi-scale direct inversion. Liver stiffness was measured by one experienced radiologist (KY) using the free-hand method, by placing region of interests (ROIs) on the stiffness map, mainly in the right hepatic lobe, avoiding apparent pathologies, large vessels, areas with inadequate wave propagation and cross-hatching marks [14]. An average of the four slices was used to represent the liver stiffness of each patient. These data were recorded at the time of routine clinical practice and liver stiffness measurement was not repeated for this study

*Pathological assessment*

The surgically resected or percutaneously biopsied specimens were stained with hematoxylin–eosin and Masson's trichrome, and the degree of fibrosis using the Metavir system [16, 17] was routinely described in the pathology reports. Although the Metavir system was originally designed to assess liver tissues of patients with chronic hepatitis C, it has also been applied to chronic liver disease of other various etiologies [18, 19].

*ECV calculation*

One of the authors (IE) who has 10-year experience as an abdominal radiologist and was blinded to MRE or pathological results, placed free-hand ROI on the two iodine material density maps, namely, iodine(-water), and iodine(-blood) density maps. An ROI, as large as possible, was placed for the liver in the right lobe, avoiding apparent pathologies, post-therapeutic changes, vessels, and artifacts.

ROIs for the blood pool were placed in the Ao around the level of the porta hepatis, and also in the suprahepatic IVC. An example of iodine(-water) images with prominent streaking artifacts is shown in Fig. 2. Four types of ECV, namely, first using Ao as a blood pool and water as a basis material ($ECV_{\mathbf{I–W\ Ao}}$), second using Ao as a blood pool and blood as a basis material ($ECV_{\mathbf{I–B\ Ao}}$), third using IVC as a blood pool and water as a basis material ($ECV_{\mathbf{I–W\ IVC}}$), and finally, using IVC as a blood pool and blood as a basis material ($ECV_{\mathbf{I–B\ IVC}}$), were thus calculated.

The same author (IE) placed ROIs on the unenhanced and equilibrium phase 65-keV monochromatic-equivalent images, which were considered equivalent to the single energy 120-kVp images, at the corresponding sites to the ROIs on iodine density images, and ECV was calculated in a conventional fashion ($ECV_{\mathbf{conv\ Ao}}$).

*Assessments and statistics*

We first assessed the adequacy to use blood as the basis material, instead of water. One of the authors (KS) measured the value of the Ao at the level of porta hepatis, avoiding as much artifact as possible, both on the iodine(-water) density image and iodine(-blood) images at the unenhanced phase. The mean and standard deviation were compared between the two image sets.

Then, we correlated five types of ECVs, namely $ECV_{\mathbf{conv\ Ao}}$, $ECV_{\mathbf{I\text{-}W\ Ao}}$, $ECV_{\mathbf{I\text{-}B\ Ao}}$, $ECV_{\mathbf{I\text{-}W\ IVC}}$, and $ECV_{\mathbf{I\text{-}B\ IVC}}$, to the liver stifness as measured with MRE using Pearsons' correlation test, and also to pathological degree of fibrosis using Spearman's signed rank correlation test, when available. The degree of correlation, namely $R^2$ for Pearson's correlation and rho

value for Spearman's singed rank test were compared among the five ECVs. To determine the ECV cut-of value to discriminate advanced (F3–4) from early stage (F0–2) liver fibrosis, receiver operator characteristic (ROC) analysis was employed for the ECV showing the best correlation coefcient. All statistical analyses were performed using JMP Pro13.0.0 (SAS Corporation, Cary, USA).

## Results

*Assessment of the adequacy of using blood as a basis material*

The mean value of Ao on unenhanced iodine(-water) density image was 3.71 ± 1.27 (mean ± SD) with a range from 0.84 to 6.7 and that on unenhanced iodine(-blood) density image was 0.44 ± 1.32 with a range from − 2.5 to 3.4. Bland–Altman analysis showed significant difference between the two ($p < 0.0001$, not shown).

On the other hand, standard deviation (SD) of the abdominal aorta on unenhanced iodine(-water) density image was 2.72±1.03 with a range from 1.72 to 6.76 and that on unenhanced iodine(-blood) density image was 3.61±1.40 with a range from 2.3 to 9.8. Bland–Altman analysis showed significant difference between the two (p<0.0001, not shown).

*Correlation between the five types of ECVs and liver stiffness or pathological fibrosis grades*

All five ECVs showed significant correlation with liver stiffness(kPa) as measured by MRE ($p < 0.0001$), and the correlation coefficient ($R^2$) was the highest for $ECV_{\mathbf{I-B\ IVC}}$ (0.52), and the lowest for $ECV_{\mathbf{conv\ Ao}}$ (0.25) (Table 2, Fig. 3).

Pathological data for the grades of fibrosis were available in 28 patients (surgical resection in 10, percutaneous biopsy in 18), which were obtained within 1 year from CT examinations. There were 3, 3, 4, 9, and 9 patients for fibrosis grades 0, 1, 2, 3, and 4,

187 respectively. Although all five ECVs showed significant correlation with liver fibrosis grades
188 ($p < 0.01$), $ECV_{I\text{-}B\ IVC}$ showed the highest rho (0.76) and the lowest $p$ value (< 0.0001),
189 whereas $ECV_{I\text{-}W\ Ao}$ showed the lowest rho (0.59) and the highest $p$ values (0.001) (Fig. 4).
190 $ECV_{I\text{-}B\ IVC}$ for fibrosis grades 0, 1, 2, 3, and 4, were 20.9 ± 4.6, 20.7 ± 3.1, 27.0 ± 4.8, 28.5 ±
191 6.7, and 36.4 ± 2.6%, respectively (mean ± standard deviation) (Fig. 5). Using an $ECV_{I\text{-}B\ IVC}$
192 cut-off value of 26.4%, discrimination of advanced stage (F3–4) from early stage (F0–2)
193 liver fibrosis was achieved with 78% sensitivity, 90% specificity, 82% accuracy, 93%
194 positive predictive value, and 69% negative predictive value. Area under the curve or Az
195 value of ROC analysis was 0.85 (95% confidence interval 0.67–0.93). An iodine(-water)
196 density image and iodine(-blood) density image of a representative case are shown in Fig.
197 6.
198
199 **Discussion**

200 Although several investigations have suggested the possibility of ECV as a biomarker of
201 liver fibrosis [6–9], its reported clinical utility is diverse. Bandula et al. [8] reported
202 relatively good correlation between ECV and histological fibrosis grades, with an $R^2$ value
203 of 0.64 at Pearson's correlation test, whereas Yoon et al. [9] reported weak correlation,
204 with a rho value of 0.49 at Spearman's rank correlation. One possible reason for this
205 discrepancy is the delay time used for those investigations. The former used 30 min delay
206 images which were added to the routine clinical examination, whereas the latter used
207 routine 3 min delay images. Theoretically, 3 min is very short to obtain true "equilibrium"
208 phase [10], and in our institute, equilibrium phase images are routinely obtained at 240 s
209 since 2008, and recently, Shinagawa et al. reported relatively good correlation between
210 liver ECV and liver stiffness as measured by MRE, or pathological fibrosis grades, utilizing
211 240-s equilibrium phase delay time [10]. We, therefore, consider a 240-s acquisition for
212 the equilibrium phase to be a good compromise for routine clinical practice. The optimal
213 delay time of equilibrium phase images for adequate ECV calculation, however, should be

214 investigated as a separate study, which is beyond the scope of this study.

215 For iodine material density imaging, iodine–water set has been utilized as basis materials
216 so far, and iodine–blood combination has never been reported [11, 12], to the best of our
217 knowledge. However, this iodine–water approach may result in erroneous iodine
218 quantification, which was highlighted by the fact that iodine density value of abdominal
219 aorta on the unenhanced phase was not zero, which would reasonably lead to imprecise
220 calculation of ECV. We, therefore, proposed to use iodine–blood set instead of
221 conventional iodine–water set as basis materials, and obtained favorable results, namely
222 close to zero value of the abdominal aorta on the unenhanced images, and better
223 correlation between ECV and reference standards (Table 2, Figs. 3, 4, 5). Because iodine(-
224 blood) density images can be easily generated by inputting blood data which can be
225 obtained from NIST site [13], its widespread use might be advantageous for any
226 quantitative analysis of iodine on DECT as compared to conventional iodine(-water)
227 density images, which should be confirmed in future studies. Unfortunately, standard
228 deviation or noise increased slightly on the iodine(-blood) density images as compared
229 to iodine(-water) density images, probably because the difference in the densities
230 between two basis materials is less for the iodine–blood set, as compared to iodine–water
231 set. Technological improvement to reduce this noise would be necessary to solve this
232 problem.

233 Another possible approach could have been simply subtracting iodine density images of
234 unenhanced phase from those of the equilibrium phase, which we did not adopt in this
235 study. Because one big merit of using DECT data is the iodine density images, which would
236 theoretically obviate the necessity of precontrast imaging, we tried to improve it by
237 proposing iodine(-blood) density map instead of conventional iodine(-water) density map,
238 to make the most of the DECT technology, and dared not to assess subtraction method in
239 this study. Recently, three-material decomposition method has been proposed [20], which
240 could be another promising alternative to solve this problem, but unfortunately, our DECT

241 does not have this capability.

242 Another problem we encountered was the streaking artifacts on the iodine density
243 images typically seen around the vertebrae which frequently affected the blood pool
244 measurement at the abdominal aorta. We, therefore, proposed to use IVC just above the
245 liver as blood pool, instead of aorta, for more consistent and appropriate measurement
246 (Table 2, Figs. 3, 4, 5, 6). Recent technological advance has enabled reduction of this type
247 of artifacts in the newer version of DECT, which may facilitate ECV calculation.

248 Our results suggested that correlation of $ECV_{I\text{-}B\ IVC}$ with pathological fibrosis grades seems
249 at least comparable to those of previously reported ECVs calculated from 10 min
250 equilibrium phase data [6–8]. With the usage of iodine(-blood) density images obtained
251 from 240 s equilibrium phase DECT data, degree of liver fibrosis can be assessed within
252 the routine clinical diagnostic CT examination without adding any extra scan time or
253 radiation, which would benefit patients with chronic liver diseases. In contrast, correlation
254 with liver stiffness measured by MRE was rather poor, as compared to the results
255 reported by Shinagawa et al. [10]. This may at least partly be attributable to small number
256 of subjects, or different patient population. Similarly, the reason why $ECV_{conv\ Ao}$ performed
257 so poorly in the correlation with MRE ($R^2$ = 0.25) might at least in part be anatomical
258 misregistration between precontrast and equilibrium phase images.

259 Limitations of the present study include its retrospective nature and the small number of
260 subjects, particularly those with pathological confirmation. We used MRE as surrogate
261 reference standard to pathology, but further prospective studies using larger number of
262 pathologically proven subjects should be performed to validate our results. Second, as
263 mentioned above, the optimal equilibrium phase delay time is not determined and should
264 be explored as a separate study. Third, because several pathologists were involved in
265 reporting the degree of fibrosis in daily practice, the criteria in assessing the pathological
266 degree of fibrosis might have been inconsistent. Forth, although we obtained different
267 correlation coefficients for five ECVs, namely $R^2$ and rho values, we could not assess its

268 statistical significance because our software does not allow such analyses. .
269

270 **Conclusion**

271 $ECV_{I-B\ IVC}$, calculated from routine clinical diagnostic DECT equilibrium phase data alone,
272 obtained with a delay time of 240 s, showed better correlation to liver stiffness as
273 measured by MRE and pathological fibrosis grades than other ECVs, which could be a
274 promising biomarker of liver fibrosis.
275

## References


1. Martinez SM, Crespo G, Navasa M, Forns X (2011) Noninvasive assessment of liver fibrosis. Hepatology 52:325–335.
2. Venkatesh SK, Yin M, Ehman RL (2013) Magnetic Resonance Elastography of Liver: Technique, Analysis, and Clinical Applications. J. Magn. Reson. Imaging 37:544–555.
3. Tang A, Cloutier G, Szevereny NM, Sirlin CB (2015) Ultrasound Elastography and MR Elastography for Assessing Liver Fibrosis: Part 1, Principles and Techniques. *AJR* 205:22–32
4. Tang A, Cloutier G, Szevereny NM, Sirlin CB (2015) Ultrasound Elastography and MR Elastography for Assessing Liver Fibrosis: Part 2, Diagnostic Performance, Confounders, and Future Directions. *AJR* 205:33–40
5. Yoshimitsu K, Mitsufuji T, Shinagawa Y, et al (2016) MR elastography of the liver at 3.0 T in diagnosing liver fibrosis grades; preliminary clinical experience. Eur Radiol 26(3):656-63.
6. Varenika VJ, Fu YJ, Maher JJ,et al (2013) Hepatic Fibrosis: Evaluation with Semiquantitative Contrast-enhanced CT. Radiology 266:151–158
7. Zissen MH, Wang ZJ, Yee J, Aslam R, Monto AM, Yeh BM (2013) Contrast-Enhanced CT Quantification of the Hepatic Fractional Extracellular Space: Correlation With Diffuse Liver Disease Severity. *AJR* 201:1204–1210
8. Bandula S, Punwani S, Rosenberg WM, et al (2015) Equilibrium Contrast-enhanced CT Imaging to Evaluate Hepatic Fibrosis: Initial Validation by Comparison with Histopathologic Analysis. Radiology 275:136–143
9. Yoon JH, Lee JM, Klotz E, et al (2015) Estimation of Hepatic Extracellular Volume Fraction Using Multiphasic Liver Computed Tomography for Hepatic Fibrosis Grading. Invest Radiol 50: 290-296.

10. Shinagawa Y, Sakamoto K, Sato K, et al (2018) Usefulness of new subtraction algorithm in estimating degree of liver fibrosis by calculating extracellular volume fraction obtained from routine liver CT protocol equilibrium phase data: preliminary experience. *EJR* 103:99-104
11. McCollough CH, Leng S, YU L, et al (2015) Dual-and Multi-energy CT: principles, technical approaches, and clinical applications. Radiology 276:637-653
12. Ep T, Le O, Liu X, et al (2017) "How to" incorporate DE imaging into a high volume abdominal imaging practice. Abdom Radiol 42:688-701
13. https ://physi cs.nist.gov/PhysR efDat a/Xcom/html/xcom1 .html. Accessed 30 Aug 2019.
14. Mitsufuji T, Shinagawa Y, Fujimitsu R et al (2013) Measurement repeatability of MR elastography at 3.0T: comparison among three different region-of-interest placement methods. Jpn J Radiol 31: 336–341
15. Shinagawa Y, Mitsufiji T, Morimoto S et al (2014) Optimization of scanning parameters for MR elastography at 3.0 T clinical unit: volunteer study. Jpn J Radiol 32:441–446
16. The French METAVIR Cooperative Study Group (1994) Intraobserver and interobserver variations in liver biopsy interpretation inpatients with chronic hepatitis C. Hepatology 20:15–20
17. Bedossa P (1996) An algorithm for the grading of activity in chronic hepatitis C. Hepatology 24:289–293
18. Foucher J, Chanteloup E, Vergniol J et al (2006) Diagnosis of cirrhosis by transient elastography (FibroScan): a prospective study. Gut 55:403–408
19. Brunt EM (2000) Grading and staging the histopathological lesions of chronic hepatitis: the Knodell histology activity index and beyond. Hepatology 31:241–246
20. https://www.innervision.co.jp/suite/siemens/technote/080408/index.html. Accessed 30 Aug 2019.

**Figure Legends**

Fig.1 Patient selection flowchart.

Fig.2 An example of prominent streaking artifacts from vertebral bodies in a 76 year-old man with hepatitis C viral infection.

2A: Iodine(-water) density image around the porta hepatis. Severe streaking artifact is evident overlapping the abdominal aorta (arrow).

2B: Iodine(-water) density image 3 cm cephalad to Fig.2A. Note the inferior vena cava is almost free of artifact (arrow).

Fig.3 Correlation between the liver stiffness in kPa as measured by MR elastography and ECV obtained using iodine and blood as the basis materials and inferior vena cava as a blood pool ($ECV_{I\text{-}B\ IVC}$). $ECV_{I\text{-}B\ IVC}$ =19.1 + 1.86 kPa, was obtained, with correlation coefficient $R^2$ of 0.52 ($p<0.0001$).

Fig.4 Correlation between pathological fibrosis grades (F-grade) and five types of extracellular volume fractions (ECVs). ECV obtained using iodine and blood as the basis materials and inferior vena cava as a blood pool ($ECV_{I\text{-}B\ IVC}$) showed the highest rho (0.76) and lowest p values (<0.0001) at Spearman's rank correlation test, as compared to other four types of ECVs, namely, ECV measured by manually placed region-of-interests ($ECV_{conv\ Ao}$) (rho=0.61, p=0.0008), ECV obtained using iodine and water as the basis materials and aorta as a blood pool ($ECV_{I\text{-}w\ Ao}$) (rho=0.59, p=0.001), ECV obtained using iodine and water as the basis materials and inferior vena cava as a blood pool ($ECV_{I\text{-}w\ IVC}$) (rho=0.68, p<0.0001), and ECV obtained using iodine and blood as the basis materials and aorta as a blood pool ($ECV_{I\text{-}B\ Ao}$) (rho=0.71, p<0.0001).

Fig.5 Extracellular volume fraction, obtained using blood as one of the basis materials and inferior vena cava as a blood pool ($ECV_{I\text{-}B\ IVC}$), for each grade of pathological liver fibrosis. Significant differences were present between F4 and F0-3 (Tukey-Kramer HSD test). Using a cutoff value of 26.4 %, discrimination of advanced stage (F3-4) from early stage (F0-2) liver fibrosis was achieved with 78% sensitivity, 90% specificity, 82% accuracy, 93% positive predictive value, and 69% negative predictive value. Az value was 0.85.

Fig.6 Equilibrium phase iodine (-water) (6A) and iodine (-blood) (6B) density images of a 64-year-old man with hepatitis C viral infection. Note more noises in the latter than in the former.

Table 1 Demographic data of the patients

| | |
|---|---|
| **sex** | **M : F = 26 : 26** |
| **age** | **35-88 years old (mean 66.8)** |
| **background** | **HBV/HCV/NBNC/ALD/noLD/others = 11/24/3/1/11/2** |
| **Child-Pugh score** | **normal or 5/6/7/8/9 = 37/6/5/2/2** |
| **liver stiffness at MR elastography (kPa)** | **1.1-11.4 kPa (mean 5.0)** |
| **pathological F grades (n=28）** | **F0/ F1/ F2/ F3/ F4 = 3/ 3/ 4/ 9/ 9** |

M/F: male/female, HBV/HVC: hepatitis B/C viral infection, NBNC: non-B non-C liver disease, ALD: alcoholic liver disease, noLD: no liver disease

Table 2 Correlation between 5 extracellular volume fractions and liver stiffness (kPa).

| Types of ECV | equation | $R^2$ | p value |
|---|---|---|---|
| $ECV_{conv\ Ao}$ | 25.3 + 1.14*kPa | 0.25 | 0.0001 |
| $ECV_{I\text{-}W\ Ao}$ | 24.2 + 1.37*kPa | 0.34 | <0.0001 |
| $ECV_{I\text{-}B\ Ao}$ | 19.0 + 1.56*kPa | 0.44 | p<0.0001 |
| $ECV_{I\text{-}W\ IVC}$ | 24.8 + 1.59*kPa | 0.39 | p<0.0001 |
| $ECV_{I\text{-}B\ IVC}$ | 19.1 + 1.86*kPa | 0.52 | p<0.0001 |

$ECV_{conv\ Ao}$ : extracellular volume fraction (ECV) calculated in a conventional method, namely, by placing region-of-interest in the unenhanced and equilibrium phase 65 keV (equivalent to 120kVp images) monochromatic images.

$ECV_{I\text{-}W\ Ao}$: ECV calculated from iodine (-water) density images, using aorta at the porta hetatis level as blood pool.

$ECV_{I\text{-}B\ Ao}$: ECV calculated from iodine (-blood) density images, using aorta at the porta hetatis level as blood pool.

$ECV_{I\text{-}W\ IVC}$: ECV calculated from iodine (-water) density images, using inferior vena cava (IVC) just above the diaphragm as blood pool.

$ECV_{I\text{-}B\ IVC}$: ECV calculated from iodine (-blood) density images, using inferior vena cava (IVC) just above the diaphragm as blood pool.

**Fig.1**

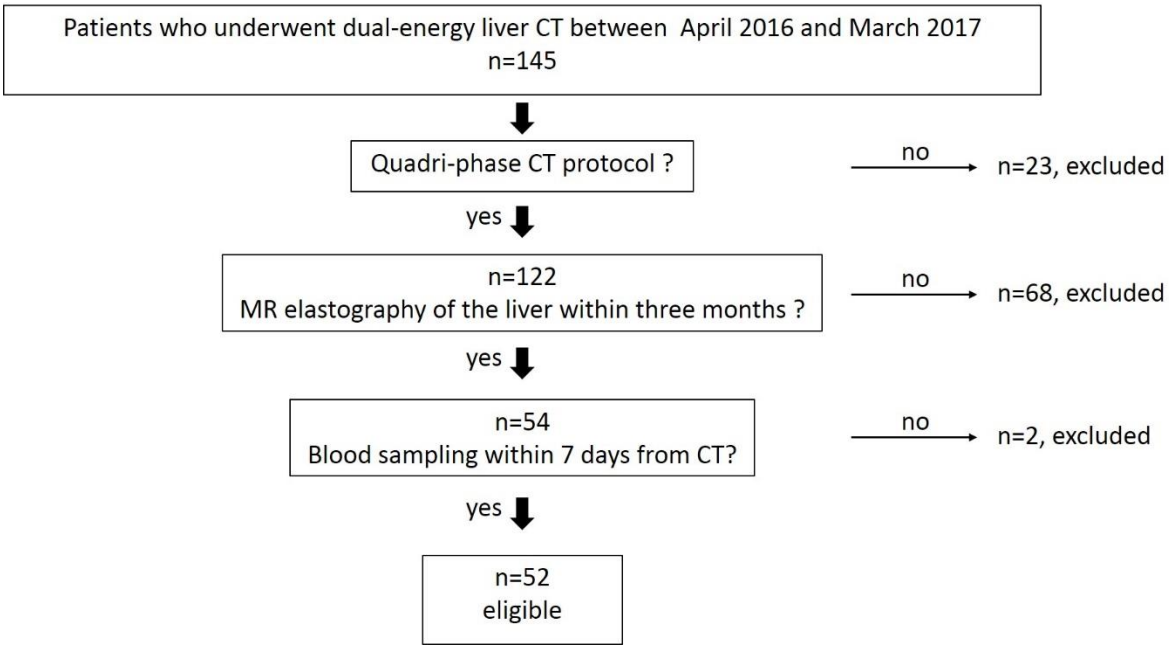
Patients who underwent dual-energy liver CT between April 2016 and March 2017
n=145
Quadri-phase CT protocol ?
no
n=23, excluded
yes
n=122
MR elastography of the liver within three months ?
no
n=68, excluded
yes
n=54
Blood sampling within 7 days from CT?
no
n=2, excluded
yes
n=52
eligible

**Fig.2A**

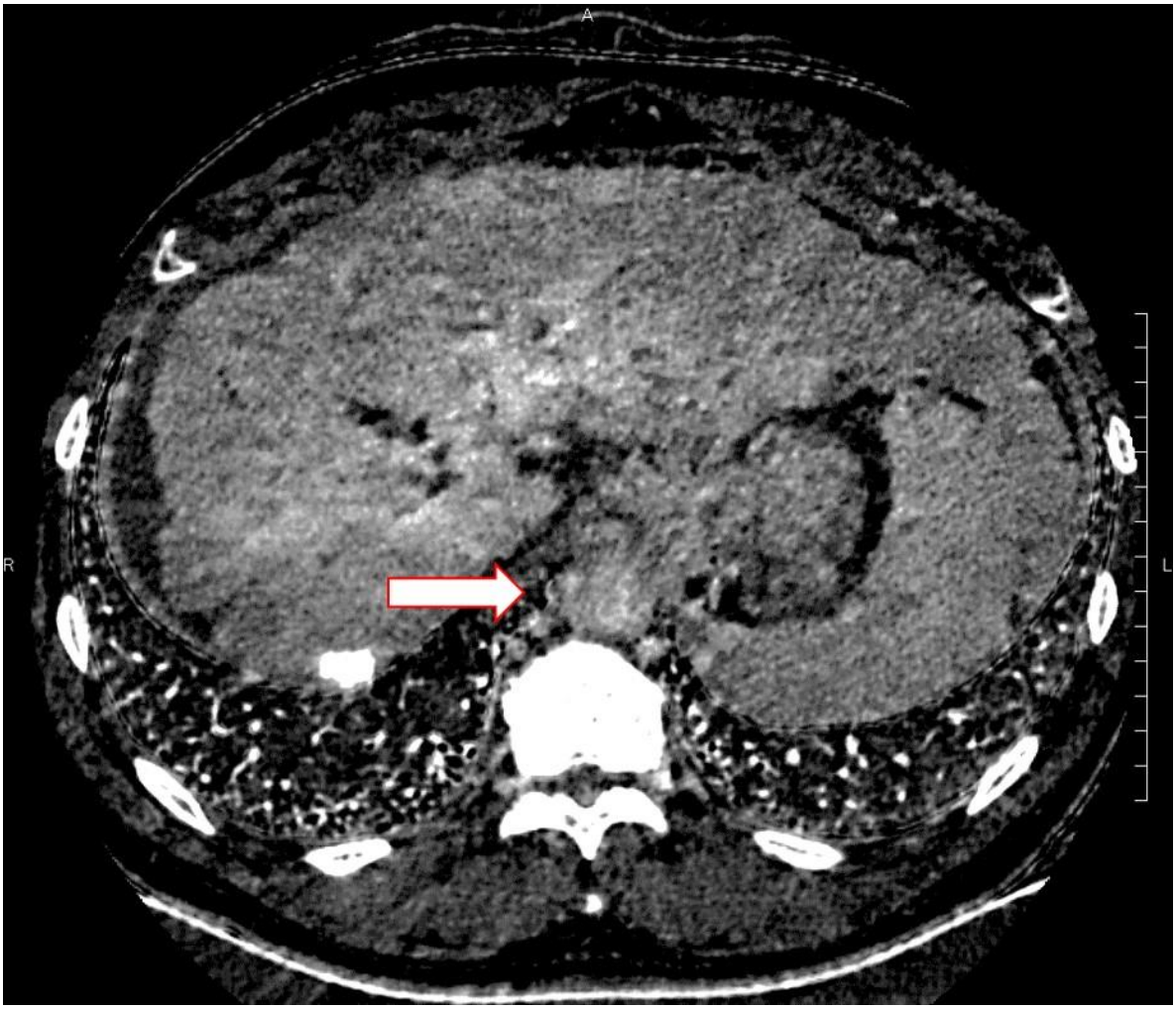

**Fig.2B**

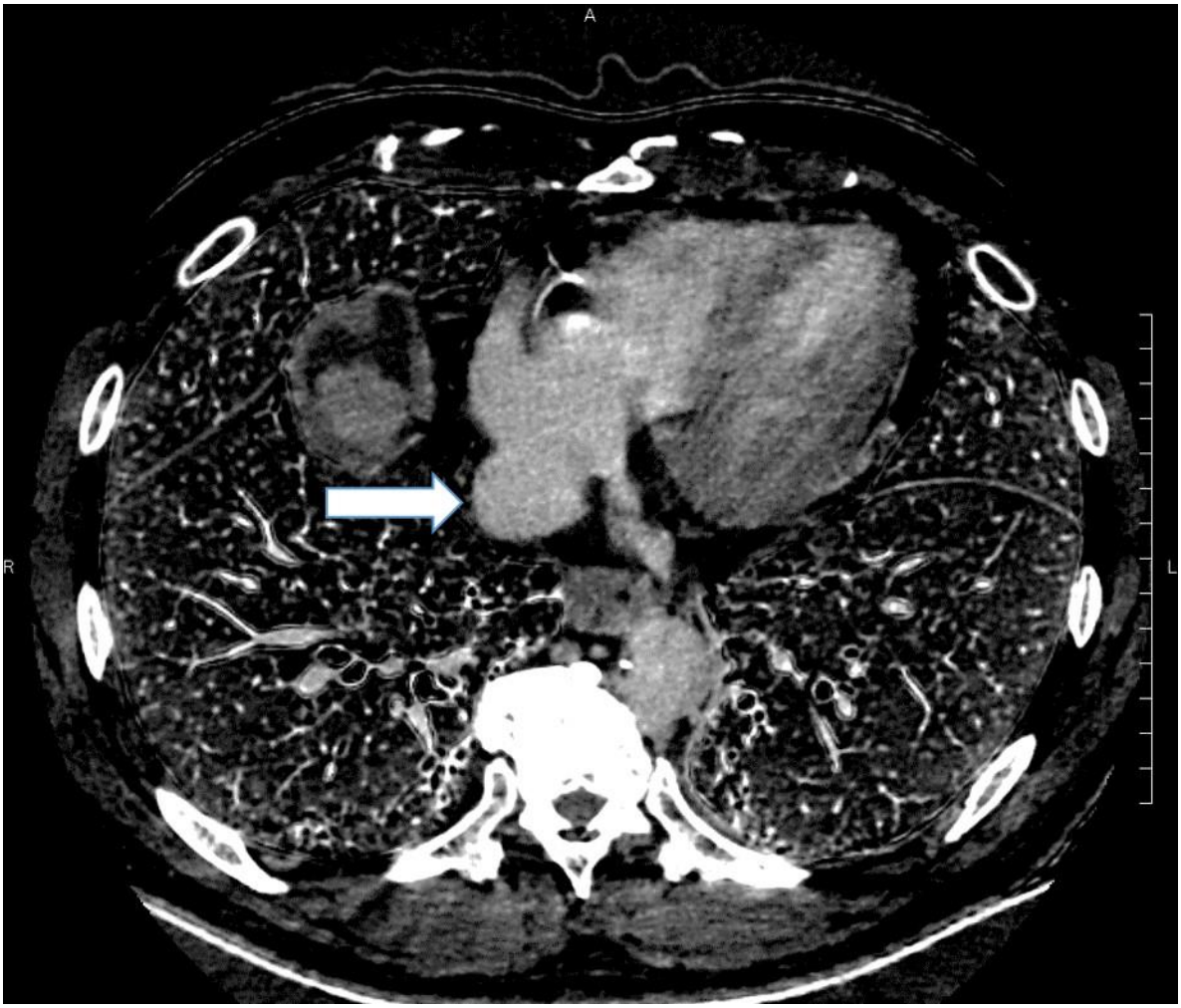

**Fig.3**

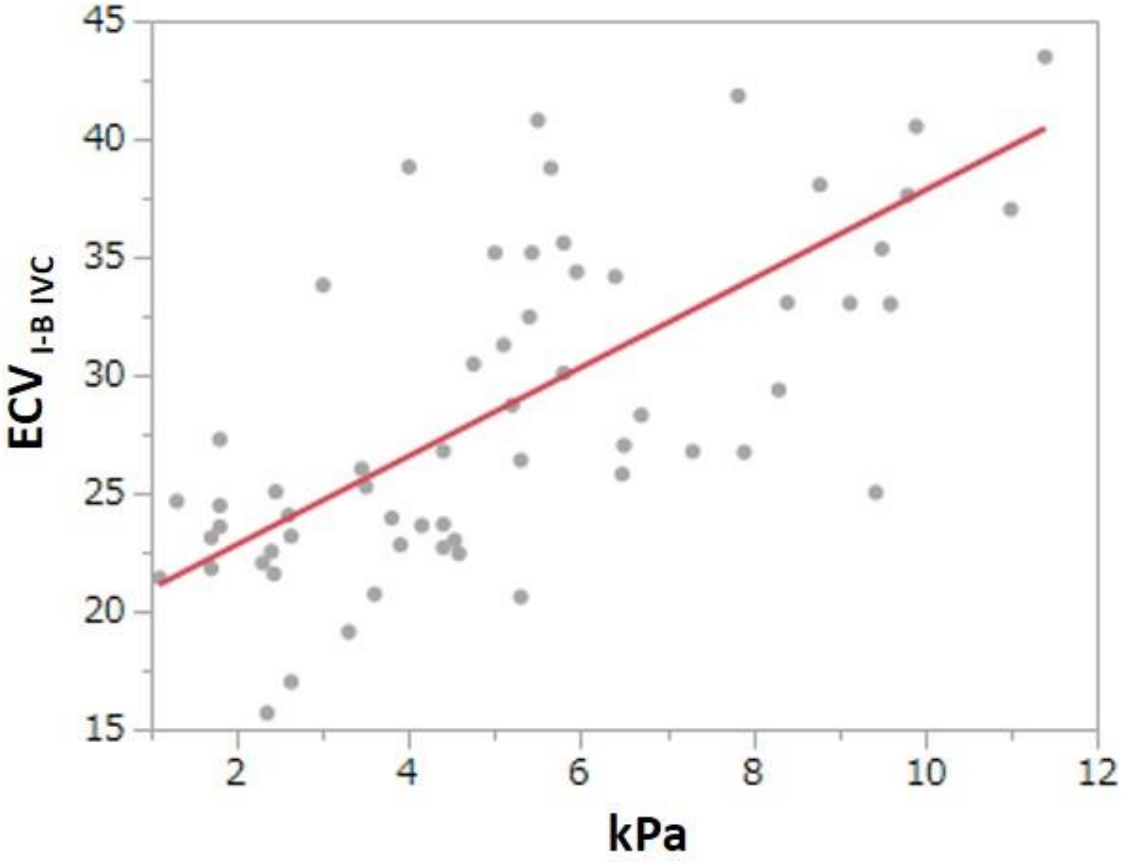

**Fig.4**

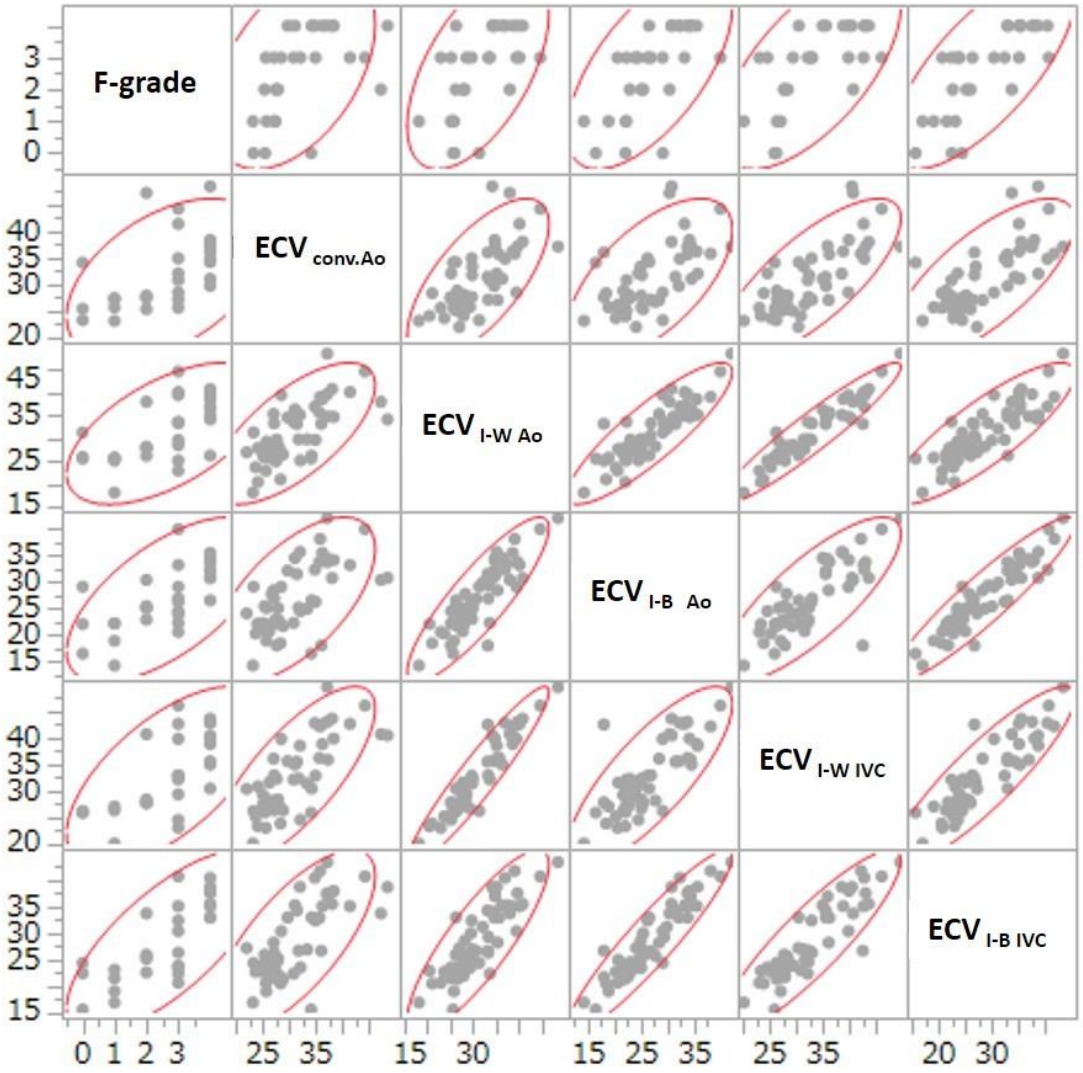


| vs F-grades | Rho value | P value |
|---|---|---|
| ECV conv Ao | 0.61 | 0.0008 |
| ECV I-W Ao | 0.59 | 0.001 |
| ECV I-B Ao | 0.71 | <0.0001 |
| ECV I-W IVC | 0.68 | <0.0001 |
| ECV I-B IVC | 0.76 | <0.0001 |

**Fig.5**

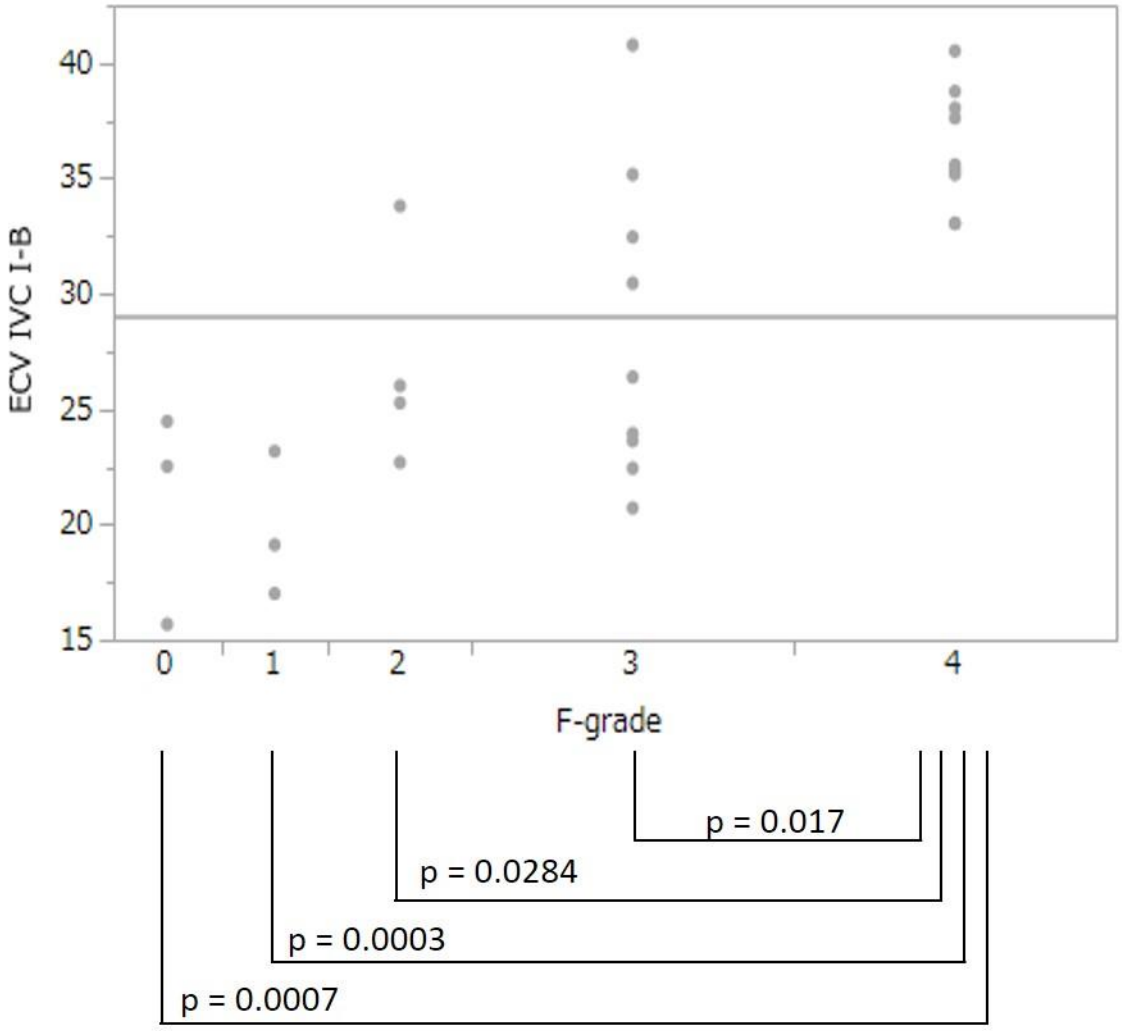
ECV IVC I-B
40
35
30
25
20
15
0
1
2
3
4
F-grade
p = 0.017
p = 0.0284
p = 0.0003
p = 0.0007

**Fig.6A**

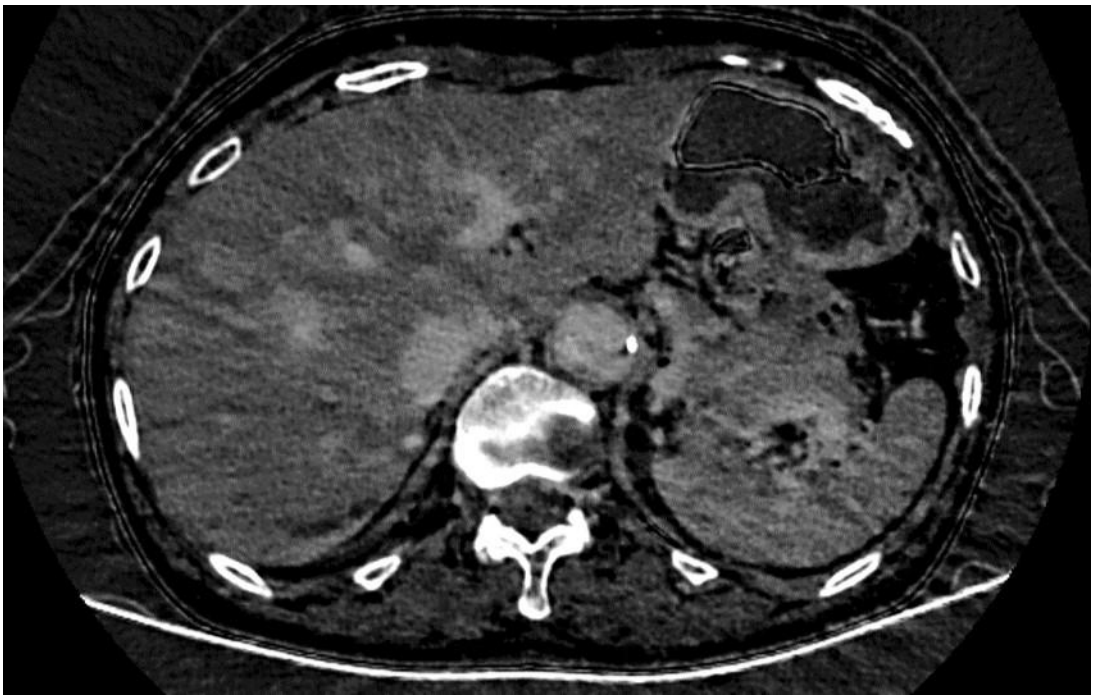

**Fig.6B**